Journal of Alloys and Compounds 471 (2009) 190–196

Contents lists available at ScienceDirect

Journal of Alloys and Compounds

journal homepage: www.elsevier.com/locate/jallcom

Comparative study of synthesis and characterization of monodispersed SiO_2 @ Y_2O_3:Eu^{3+} and SiO_2 @ Y_2O_3:Eu^{3+} @ SiO_2 core–shell structure phosphor particles

Yuan-Xiang Fu, Yan-Hui Sun*

School of Chemistry and Environment, South China Normal University, Guangzhou 510006, PR China

ARTICLE INFO

Article history:
Received 24 January 2008
Received in revised form 9 March 2008
Accepted 12 March 2008
Available online 29 April 2008

Keywords:
Coating materials
Rare earth alloys and compounds
Precipitation
Optical properties
Luminescence

ABSTRACT

Monodispersed SiO_2 @ Y_2O_3:Eu^{3+} and SiO_2 @ Y_2O_3:Eu^{3+} @ SiO_2 nanospheres contain SiO_2 as core and Y_2O_3:Eu^{3+} as shell or another SiO_2 shell coated on the surface of SiO_2 @ Y_2O_3:Eu^{3+} particles were synthesized, respectively. The synthesis of core–shell particles SiO_2 @ Y_2O_3:Eu^{3+} involved the SiO_2 core ultrasonically dispersed into a certain amount of polyethylene glycol solution, and the deposition of Y_2O_3:Eu^{3+} on the surface of SiO_2 core through homogeneous precipitation of Y^{3+} and Eu^{3+} using urea as precipitator. More over, the particles SiO_2 @ Y_2O_3:Eu^{3+} as core was ultrasonically dispersed into a certain amount of ethanol and followed by sol–gel processing of tetraethoxysilane to form another silica shell. The morphology structures and sizes of the resulting particles were analyzed by SEM and TEM, which indicated that the resulting particles dispersed regularly and the microstructures of the particles are clearly core–shell or core–shell–shell structures. XRD patterns characterized the crystal structures of deposited Y_2O_3:Eu^{3+} shell or SiO_2 shell after heat treatment at 900 °C. Photoluminescence determination showed that both the phosphors can be excited by ultra violet at 254 nm which showed red-shift. Under the excitation at 254 nm, the Eu^{3+} ion mainly shows its characteristic red (612 nm, $^5D_0$–$^7F_2$) emission in the particles from Y_2O_3:Eu^{3+} shell. The emission intensity of Eu^{3+} was affected by the SiO_2 core or shell in some extent.

1. Introduction

Recently, the synthesis of core–shell nanostructures has emerged as an attractive research area in material chemistry since the morphology and the size of the core–shell materials can be tailored easily by changing the core materials' shape, size or the shell's thickness [1]. More over, coating relative inexpensive cores with the expensive shell materials or coating expensive shells on the inexpensive cores materials can lower the cost of the functional materials [2]. Especially, the shell material such as SiO_2 with an optical transparency can protect the surface of the functional materials such as the noble metals, magnetic compounds and phosphor materials from contaminating by some impurity in surroundings [3].

Silica is frequently used in core–shell structured materials, as either a core or a shell because of their inexpensiveness, easiness to get spherical particles with narrow size distribution, chemical inertness, and optical transparency [3]. If the silica spheres are coated with phosphor layers, a kind of core–shell phosphor materials with spherical morphology will be obtained, and the size of the phosphor particles can be controlled by the size of the silica core or the thickness of the shell and the number of coating cycles. Coating particles with silica as a shell is a promising strategy which presents several advantages especially in the field of biological and imaging applications. Apart ensuring core protection and water-solubility, the silica shell realizes two crucial functions. The first consists in allowing functionalization by biological groups since silica can be derived by organoalkoxysilanes containing reactive organic groups (e.g. amine, thiol and isothiocyanate). The second is increasing the optical response of luminescing cores used as optical tags [3].

It is well known that europium-doped Y_2O_3 phosphor (Y_2O_3:Eu^{3+}) has been widely used in lighting and cathode ray tubes as a red-emitting phosphor [4]. Recent researches have indicated that it is also the promising candidate for field emission display (FED) devices [5]. For the FED applications, it is highly desirable to offer spherical phosphors with controllable diameters and narrow size distributions [6]. For that purpose, core–shell particles have attracted a great deal of interest because of their difference from those of single-component materials [7–9]. The controlled coating of particles with homogeneous and organized layers without aggregation remains a challenge for material scientists. Spherical morphology of the phosphor is good for high brightness and high resolution. Additionally, high packing densities and low scattering of light can also be obtained by using spherical phosphors. So far,

* Corresponding author.
E-mail address: sunyanhui0102@163.com (Y.-H. Sun).

0925-8388/$ – see front matter © 2008 Elsevier B.V. All rights reserved.
doi:10.1016/j.jallcom.2008.03.055

many synthetic routes have been developed to control the size and distribution of phosphor particles, such as spray pyrolysis [10] and urea homogeneous precipitation [11]. However, the obtained phosphor particles are still far from the ideally monodisperse spherical morphology. On the other hand, the chemical properties of the phosphor material usually are unstable, the surface of the phosphor material has many unsaturated bond and easily absorbed some impurity which cut down the luminescence property of the phosphors [3]. So coating some shells on the surface of phosphor materials is essential in precondition of not affected the photoluminescence.

Up to now, there are many investigations of phosphor materials coated on the SiO_2 core and resulting the SiO_2 @ Y_2O_3:Eu^{3+} [7–9], SiO_2 @ YBO_3:Eu^{3+} [12], SiO_2 @ YVO_4:Dy^{3+}, Sm^{3+} [13], SiO_2 @ YAG:Ce^{3+}, Tb^{3+} [14] and so on, while there are few investigations involves the coating of SiO_2 shells on the surface of phosphors. Much investigations for SiO_2 as shells are focused on the metal or magnetic materials such as Fe_2O_3 @ SiO_2 [15], Ag @ SiO_2 [16], Au @ SiO_2 [17] and so on.

Very recently, the synthesis and application of multilayered nanostructures containing multiple shells also have begun to draw attention in synthesis of noble metal core–shell structures such as SiO_2 @ Ag @ SiO_2 [18] and SiO_2 @ Au @ SiO_2 [19]. While the presence of multiple nanoparticles anchored on solid substrates in close proximity could result in unique magnetic and optical coupling [20], the encapsulation of metal or phosphor nanoparticles by SiO_2 as in such core–shell–shell nanostructures could also provide an alternative way to increase the metal or phosphors nanoparticles' stability from aggregation or possible thermal coalescence at higher temperatures [21].

Despite their unique properties and promising potential applications, to the best of our knowledge, there are few investigations on the synthesis of core–shell–shell nanostructure have been reported on the phosphor materials so far.

In this paper, we reported a detail synthesis of core–shell–shell nanoparticles SiO_2 @ Y_2O_3:Eu^{3+}@ SiO_2 containing a silica core, Y_2O_3:Eu^{3+} nanoparticles shell and a second silica shell with a tunable size around the surface of Y_2O_3:Eu^{3+}, and characterized their structure, morphology and photoluminescence property. As a comparison, the synthesis of core–shell phosphor particles of SiO_2 @ Y_2O_3:Eu^{3+}, the pure Y_2O_3:Eu^{3+} powder phosphors are reported too.

2. Experimental

The starting materials used in the experiments were tetraethoxysilane (TEOS, 28% SiO_2, Tianjin No. 1 Chemicals Co., Ltd.), Y_2O_3 and Eu_2O_3 (99.99%, Shanghai Yuelong Nonferrous Metals Ltd.), NH_4OH (25 wt.%, A.R., Guangzhou Donghong Chemicals Co., Ltd.), HNO_3 (A.R., Guangzhou Donghong Chemicals Co., Ltd.), polyethylene glycol (PEG, molecular weight 10,000, A.R., Sanland-Chem. Inernational Incorp.) and ethanol (A.R., Guangzhou Donghong Chemicals Co., Ltd.).

2.1. Synthesis of silica cores

Monodispersed silica spheres were prepared with the procedure originally described by Stöber et al. [22] except that the reaction condition was changed in some aspects, i.e., hydrolysis of TEOS in an ethanol solution containing water and ammonia. In a typical experiment, 5 mL TEOS was added to 75 mL ethanol solution of water and ammonia. The 80 mL mixture solution containing 0.279 mol/L TEOS, 2.55 mol/L H_2O, and 1.15 mol/L ammonia was stirred at 29 °C for 4 h. The resulting silica spheres were centrifugally separated from the suspension and ultrasonically washed with distilled water and ethanol.

2.2. Coating of SiO_2 cores with Y_2O_3:Eu^{3+} shells

A certain amount of Y_2O_3 and Eu_2O_3 powders were, respectively, dissolved in excessive nitric acid to form $Y(NO_3)_3$ and $Eu(NO_3)_3$ solutions. A certain quantity of silica spheres (0.3 g) was ultrasonically dispersed in 100 mL aqueous solution containing yttrium nitrate (2×10^{-2} mol/L), europium nitrate (1.2×10^{-3} mol/L), urea (2 mol/L) and certain amount of PEG. The dispersions were then aged at 92 °C under continuous stirring for 3 h. The resulting precursors were separated by centrifugation, washed by distilled water and ethanol for several times, and then dried at 100 °C for 4 h. At last, the samples were heated at 900 °C in air for 3 h to produce the final particles SiO_2 @ Y_2O_3:Eu^{3+}.

2.3. Synthesis core–shell–shell particles SiO_2 @ Y_2O_3:Eu^{3+} @ SiO_2

A certain quantity of SiO_2 @ Y_2O_3:Eu^{3+} spheres obtained from the above step were ultrasonically dispersed in 40 mL ethanol, and then 4 mL TEOS, 10 mL ammonia and 8 mL distilled water were added into the reaction vessel in subsequently. After addition, the reaction lasted for 8 h at 40 °C under vigorous stirring. Then the resulting precursors were separated by centrifugation, washed by distilled water and ethanol for several times, and then dried at 100 °C for 4 h. At last, the samples were heated at 900 °C in air for 3 h to produce the final particles.

2.4. Coating mechanism

The silica submicrospheres prepared by the Stöber method possess an interesting substrates for the deposition of metals, oxides and functional polymers due to the narrow size distribution, the easily modified surface with silanol composition and extent of hydrogen bonding, and the isotropic interactions in an aqueous or organic suspension help to form ordered arrays on substrates [23]. The homogeneous precipitation method is a simple method for prepare monodispersed colloidal particles and uniform coated particles. In this manuscript, a continuous europium-doped yttrium oxide shell was coated on the surface of nanometer spherical silica by a homogeneous precipitation method, which leads to obtain SiO_2 @ Y_2O_3:Eu^{3+} core–shell submicrospheres. Further more, the obtained particles SiO_2 @ Y_2O_3:Eu^{3+} as core were ultrasonically dispersed into a certain amount of ethanol and followed by sol–gel processing of tetraethoxysilane to form another silica shell to obtain the core–shell–shell particles SiO_2 @ Y_2O_3:Eu^{3+} @ SiO_2. The schematic representation of the precipitation method for preparing SiO_2 @ Y_2O_3:Eu^{3+} core–shell submicrospheres and SiO_2 @ Y_2O_3:Eu^{3+} @ SiO_2 particles are given in Schemes 1 and 2.

The surface Si–OH groups play an important role for bonding the metal ions (Y, Eu) and the –NH_2 groups in urea from the coating precursor and forming the $(Y_{1-x}Eu_x)_2(OH)CO_3$ compounds on the SiO_2 surfaces in the following surface reaction process when heating the solution to 92 °C in which the urea began to decompose to NH_4OH and H_2CO_3. Further more, in the following annealing process, the compounds $(Y_{1-x}Eu_x)_2(OH)CO_3$ decomposed into Y_2O_3:Eu^{3+} and deposited on the surface of SiO_2. In this way, the core–shell structured SiO_2 @ Y_2O_3:Eu^{3+} materials have been obtained, and the whole process is shown in Scheme 1.

In the precursor solution, polyethyleneglycol (PEG, molecular, 10,000) is added as across—linking agent, the two –OH groups in PEG can connect with the –NH_2

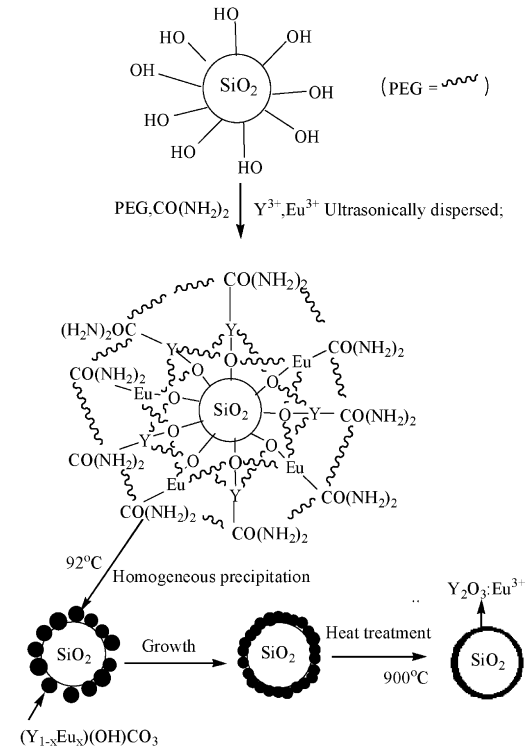

Scheme 1. Formation process of SiO_2 @ Y_2O_3:Eu^{3+} core–shell particles.

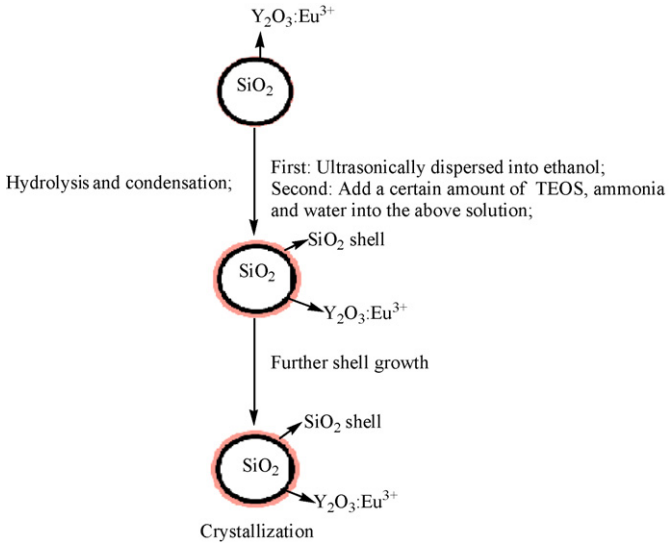

Scheme 2. Formation process of SiO_2 @ Y_2O_3:Eu^{3+} @ SiO_2 core–shell–shell particles.

groups in urea via hydration and making them more homogeneously distributed in the solution. The PEG concentration will affect the viscosity of the precursor solution. Low viscosity of the solution will result in easy deposition of a thin layer of Y_2O_3:Eu^{3+} on the SiO_2 particles, and proper increasing of the solution viscosity can increase the thickness of Y_2O_3:Eu^{3+} layer [13].

2.5. Characterization of the particles

The X-ray diffraction (XRD) of the powder samples was examined on a Rigaku-Dmax 2500 diffractometer using Cu Kα radiation λ = 0.15405 nm). The morphologies of SiO_2 @ Y_2O_3:Eu^{3+} and SiO_2 @ Y_2O_3:Eu^{3+} @ SiO_2 submicrospheres produced were observed using Quanta 400, Philips scanning electronic microscope (SEM) and transmission electron microscope (JEOL JEM-2010 (TEM)). The excition and emission spectra of samples were obtained using a Hitachi F-4500 FL Spectrophotometer with a 150 W xenon lamp.

3. Results and discussion

3.1. XRD results

X-ray diffraction patterns of bare silica spheres (a), SiO_2 @ Y_2O_3:Eu^{3+} core–shell samples (b), and SiO_2 @ Y_2O_3:Eu^{3+} @ SiO_2 samples (c) are shown in Fig. 1. The bare silica is amorphous, as evident from the presence of a broader hump in Fig. 1(a). In Fig. 1(b), SiO_2 @ Y_2O_3:Eu^{3+} core–shell sample presents three sharp peaks at

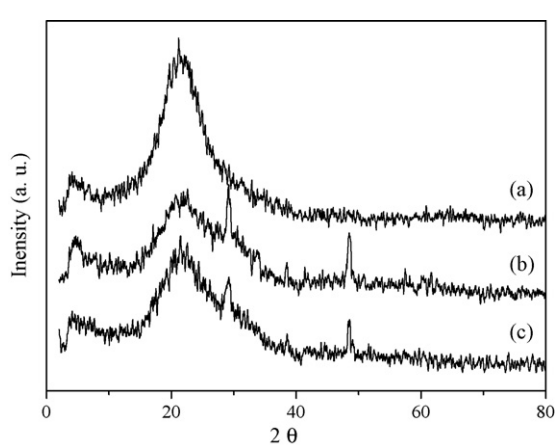

Fig. 1. X-ray diffraction patterns for SiO_2 (a), SiO_2 @ Y_2O_3:Eu^{3+} (b) and SiO_2 @ Y_2O_3:Eu^{3+} @ SiO_2 (c).

$2\theta = 29.2°$, 48.5° and 38.4°, which indicates that Y_2O_3:Eu^{3+} crystal grows well. While the other peaks of Y_2O_3:Eu^{3+} could not observed here may be enshroud by the background of SiO_2. SiO_2 @ Y_2O_3:Eu^{3+} @ SiO_2 sample in Fig. 1(c) illustrates the same patterns as that of SiO_2 @ Y_2O_3:Eu^{3+} except that the typical peaks were weak than that of SiO_2 @ Y_2O_3:Eu^{3+}. This can be explained as that the silica shell coated on the surface of the Y_2O_3:Eu^{3+}.

From the XRD patterns in Fig. 1(b) and (c), no other phase is detected which suggesting that no reaction occurred between the SiO_2 and the Y_2O_3:Eu^{3+} shells even after annealing at 900 °C. The formation of Y_2O_3:Eu^{3+} layer is due to the reaction of Y, Eu ions on silica surface at high-temperature, as shown in Scheme 1. The literature showed that if annealed at 1000 °C or higher a reaction between the Y_2O_3 shell and SiO_2 core will occur, resulting in the formation of impurity like Y_2SiO_5 phase in the samples [13]. So we limit the annealing temperature at 900 °C in this work.

In general, the nanocrystallite size can be estimated from the Scherrer formula: $D_{hkl} = K\lambda/(\beta \cos\theta)$, where λ is the X-ray wavelength (0.15405 nm), β is the full-width at half-maximum, θ is the diffraction angle, K is Scherrer constant (0.89), and D_{hkl} means the size along ($h\,k\,l$) direction. Here we take diffraction data along the (2 2 2) plane at $2\theta = 29.2°$ to calculate the size of the nanocrystallites, and the estimated average crystallite sizes of Y_2O_3:Eu^{3+} are 45 nm for pure powders, 9.85 nm for crystallite sizes of Y_2O_3:Eu^{3+} in SiO_2 @ Y_2O_3:Eu^{3+} core–shell particle and 9.42 nm for crystallite sizes of Y_2O_3:Eu^{3+} in SiO_2 @ Y_2O_3:Eu^{3+} @ SiO_2 particle, which agrees well with the results in the SEM and TEM coating shell.

3.2. SEM results

Fig. 2 shows the SEM micrographs of bare silica (a), pure Y_2O_3:Eu^{3+} (b), SiO_2 @ Y_2O_3:Eu^{3+} (c) and SiO_2 @ Y_2O_3:Eu^{3+} @ SiO_2 (d). From the SEM micrograph of Fig. 2(a), we can observed that the formed SiO_2 consists of spherical particles of average size 300 nm and these particles are non-aggregated and dispersed uniformly. In contrast, the pure Y_2O_3:Eu^{3+} powders in Fig. 2(b) contains irregular morphology particles with a wide size distribution from about 50 nm to 250 nm and these particles are aggregated obviously. After functionalizing the silica particles as core with Y_2O_3:Eu^{3+} coatings as shell, the resulting SiO_2 @ Y_2O_3:Eu^{3+} in Fig. 2(c) and SiO_2 @ Y_2O_3:Eu^{3+} particles as core with SiO_2 as another shells resulting SiO_2 @ Y_2O_3:Eu^{3+} @ SiO_2 in Fig. 2(d) still keep the morphology as the silica particle, i.e. these particles are still spherical with a smooth surface and non-aggregated. The size became larger after the coating process, it is obvious that the size is 320 nm for SiO_2 @ Y_2O_3:Eu^{3+} and about 380 nm for SiO_2 @ Y_2O_3:Eu^{3+} @ SiO_2 which agreeing well with the XRD results. It should be mentioned that minor amount of the irregular fine particles like the pure Y_2O_3:Eu^{3+} powders can be observed in Fig. 2(c) and (d). Furthermore, the dispersivity of the functionalizing particles were much uniform than that of pure Y_2O_3:Eu^{3+} powders.

3.3. TEM results

The TEM photograph of the core–shell structure SiO_2 @ Y_2O_3:Eu^{3+} in Fig. 3(a) can be observed clearly due to the different electron penetrability for cores and shells. The monodispersed SiO_2 @ Y_2O_3:Eu^{3+} spheres about 320 nm in diameter contained SiO_2 black core of 300 nm in diameter and Y_2O_3:Eu^{3+} gray color shell with an average thickness of about 10 nm can be observed from Fig. 3(a) and the magnified image of a single sphere in Fig. 3(b). Fig. 4(a) and (b) shows the uniform size distribution and clear core–shell–shell structure of SiO_2 @ Y_2O_3:Eu^{3+} @ SiO_2 particles. The SiO_2 cores are black spheres with an average size of 300 nm

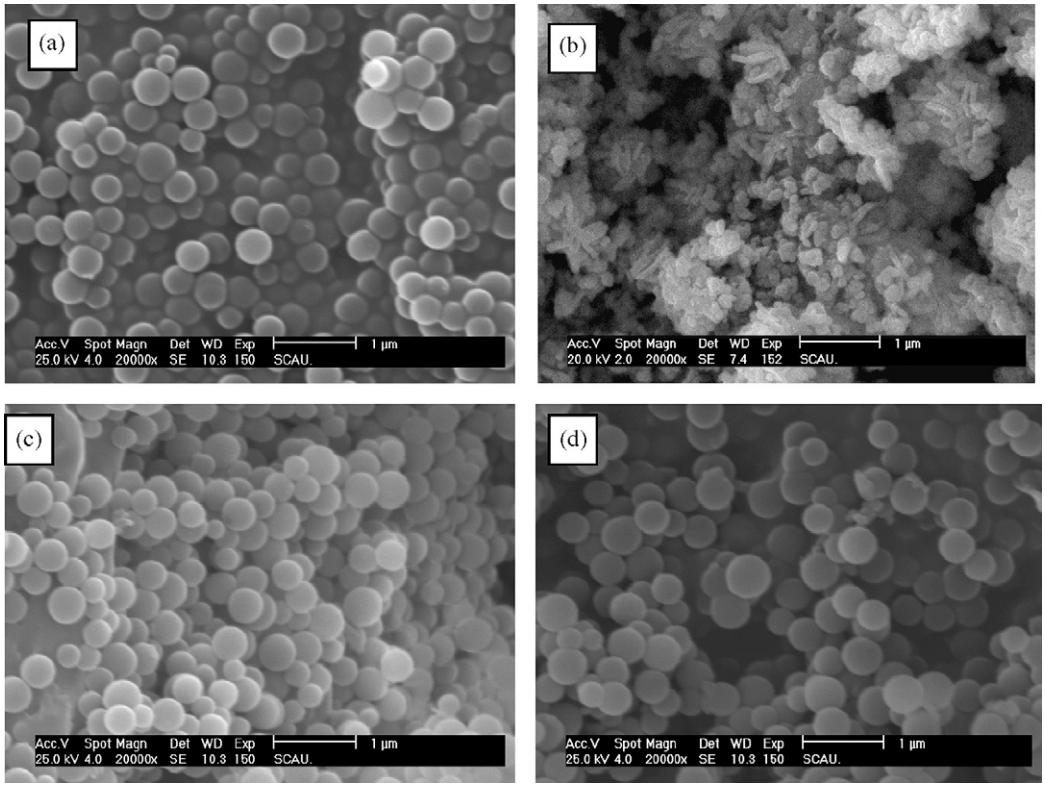

Fig. 2. SEM micrographs of SiO_2 (a), $Y_2O_3:Eu^{3+}$ (b), SiO_2 @ $Y_2O_3:Eu^{3+}$ (c) and SiO_2 @ $Y_2O_3:Eu^{3+}$ @ SiO_2 (d) samples.

in diameter, and the shell have dark color with an average thickness of 10 nm is $Y_2O_3:Eu^{3+}$ shell and the gray color with an average thickness of 30 nm is SiO_2 shell.

In addition, there are some irregular powders can be seen in Fig. 3(a) and Fig. 4(a) like that in the SEM photographs, which indicated that the coating was not completely in this study.

Fig. 5 shows the energy dispersive X-ray spectrum performed on the particles SiO_2 @ $Y_2O_3:Eu^{3+}$ @ SiO_2, and the composition analysis of the particles suggests the existence of Si (from the cores and the outside shell), O (from the cores and the shells), Y (from the inner shell) as well as Cu and C (from the Cu gridding for measurement). The Eu element was not detected clearly due to its low concentration below 5% (but it can be detected by the emission spectra, see Section 3.4). This provides additional evidence for the formation of coatings of crystalline SiO_2 @ $Y_2O_3:Eu^{3+}$ @ SiO_2 particles.

3.4. Photoluminescence properties

The excitation and emission spectra of SiO_2 @ $Y_2O_3:Eu^{3+}$ and SiO_2 @ $Y_2O_3:Eu^{3+}$ @ SiO_2 samples are shown in Figs. 6 and 7, respectively. As a comparison, the excitation and emission spectra of pure $Y_2O_3:Eu^{3+}$ was also showed in Figs. 6 and 7.

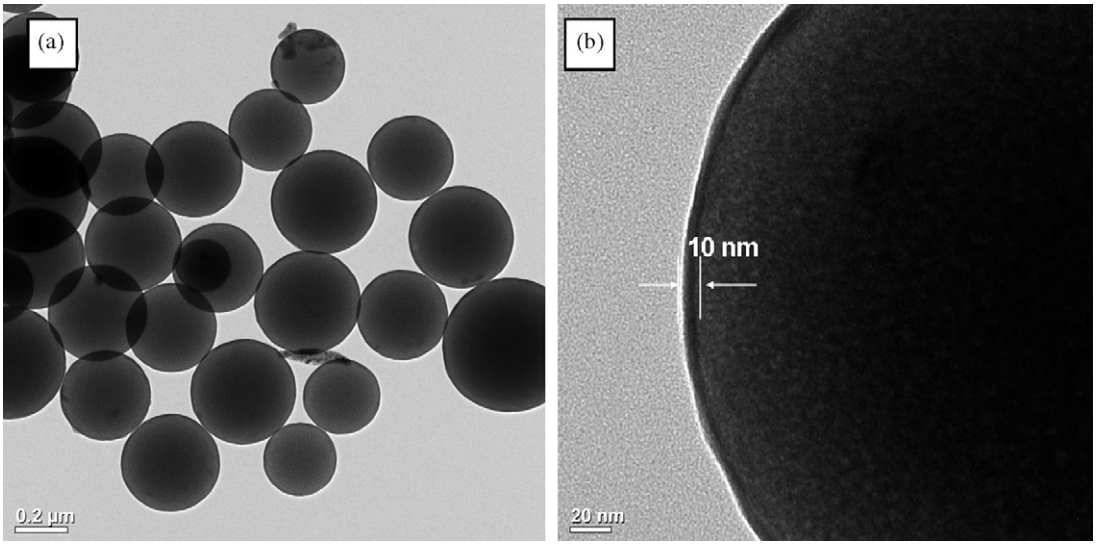

Fig. 3. TEM micrographs of core–shell nanospheres SiO_2 @ $Y_2O_3:Eu^{3+}$ (a) and the magnified image of a single sphere (b) for the samples.

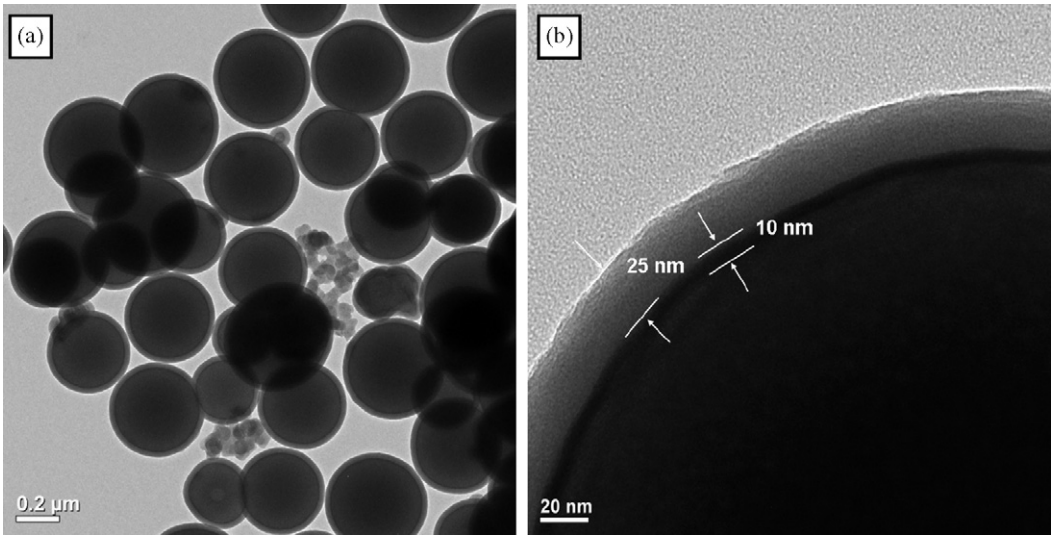

Fig. 4. TEM micrographs of core–shell–shell nanospheres SiO_2 @ Y_2O_3:Eu^{3+} @ SiO_2 (a) and the magnified image of a single sphere (b) for the samples.

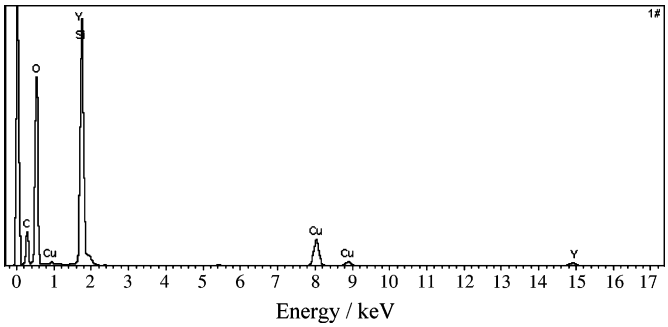

Fig. 5. Energy dispersive X-ray spectrum for the sample SiO_2 @ Y_2O_3:Eu^{3+} @ SiO_2 particles.

Here, it should be mentioned that the three PL spectra were determined in the same amount of rare earth oxide and the identical ratio of Y:Eu. That is, we used the same amount of Y^{3+} and Eu^{3+} to prepare the pure Y_2O_3:Eu^{3+} powders as that to coat the SiO_2 surfaces and to prepare the core–shell–shell particles SiO_2 @ Y_2O_3:Eu^{3+} @ SiO_2 under the complete identical conditions to the formers except that coating Y_2O_3:Eu^{3+} on the surface of SiO_2 or embeding SiO_2 @Y_2O_3:Eu^{3+} into another SO_2 shell.

The excitation spectrum was performed by monitoring the emission of Eu^{3+} $^5D_0$–$^7F_2$ transition at 612 nm. It can be seen clearly that the excitation spectrum consists of a broad band with maximum at 254 nm, which can be attributed to the charge-transfer band (CTB) between O^{2-} and Eu^{3+} [9]. Here the excitation peak is shifted toward the red from 250 nm in the pure Y_2O_3:Eu^{3+} in this study and in the literature in core–shell SiO_2 @ Y_2O_3:Eu^{3+} [9] to 254 nm in this study. We know the excitation of Eu^{3+} belongs to the charge-transfer state transition, which is related to the stability of the electron of the surrounding O^{2-} and the position of the excitation peak depends on the nature of surrounding O^{2-} ions [24]. In a crystal lattice, an O^{2-} ion is stabilized by surrounding positive ions. However, as crystallite sizes decreasing from 45 nm for pure Y_2O_3:Eu^{3+} to 9.85 nm and 9.42 nm for SiO_2 @ Y_2O_3:Eu^{3+} and SiO_2 @ Y_2O_3:Eu^{3+} @ SiO_2, respectively, the surrounding of O^{2-} ions in Y_2O_3 were changed a lot. From XRD results in Fig. 1(b) and (c), the reflection peak intensity of Y_2O_3:Eu^{3+} in the core–shell particles

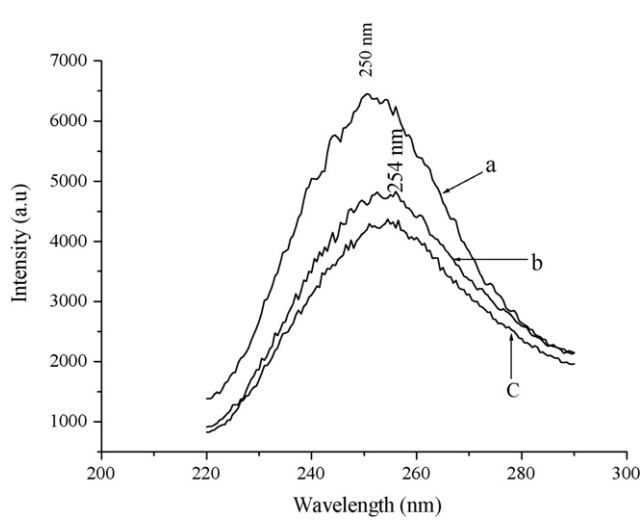

Fig. 6. Excitation spectra of Y_2O_3:Eu^{3+} (a), SiO_2 @ Y_2O_3:Eu^{3+} (b) and SiO_2 @ Y_2O_3:Eu^{3+} @ SiO_2 (c).

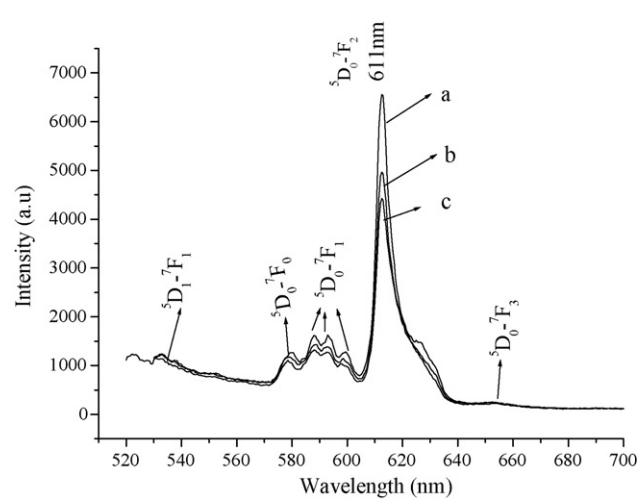

Fig. 7. Emission spectra of Y_2O_3:Eu^{3+} (a), SiO_2 @ Y_2O_3:Eu^{3+} (b) and SiO_2 @ Y_2O_3:Eu^{3+} @ SiO_2 (c).

became very weak and the width of half peak became more wide compared with that of pure $Y_2O_3:Eu^{3+}$ (the XRD pattern of pure $Y_2O_3:Eu^{3+}$ was not shown in this study). This indicated the parameter of the $Y_2O_3:Eu^{3+}$ crystal cell is more smaller. As crystallite size decreases, the surface-to-volume ratio of atoms increases and the degree of disorder of the nanostructured system increases. In that case, the O^{2-} is less stable. As a result, it requires less energy to remove an electron from an O^{2-} ion; therefore, the charge-transfer state band is shifted toward lower energy [25].

Upon excitation of the CTB at 254 nm, the obtained emission spectrum is composed of $^5D_{0,1}$–^7F_J (J = 0, 1, 2, 3) emission lines of Eu^{3+} (Fig. 7), dominated by the hypersensitive red emission $^5D_0$–$^7F_2$ transition of Eu^{3+} at 612 nm. The other emission peaks located at 535 ($^5D_1$–$^7F_1$), 579 ($^5D_0$–$^7F_0$), 589, 595, 600 ($^5D_0$–$^7F_1$), and 653 nm ($^5D_0$–$^7F_3$) are labeled in Fig. 7, which were very close to that in the pure $Y_2O_3:Eu^{3+}$ and core–shell SiO_2 @ $Y_2O_3:Eu^{3+}$ in literature [9]. In cubic $Y_2O_3:Eu^{3+}$, there are two crystallographic sites for Eu^{3+}: one is with C_2 symmetry and another with S_6 symmetry. Eu^{3+} at C_2 site contributes $^7D_0$–$^7F_{0,1,2}$ transitions to the main part of visual luminescence of $Y_2O_3:Eu^{3+}$ (580–640 nm). However, the $^5D_0$–$^7F_1$ transition lines are allowed for both C_2 and S_6 sites, are expected to arise from Eu^{3+} (C_2) and Eu^{3+} (S_6) sites simultaneously. The crystal field splitting of Eu^{3+} $^5D_0$–$^7F_{1,2}$ transitions can be seen clearly, indicating that the $Y_2O_3:Eu^{3+}$ layer is well crystallized on the surface of SiO_2 particles (agreeing well with the XRD and TEM results in Sections 3.1 and 3.3).

Further more, it can be seen that the photoluminescent intensities of the two samples (b) and (c) are affected by the addition of SiO_2 spheres both from Figs. 6 and 7. In Fig. 6, the relative excitation spectrum intensity is decreasing in the order of $Y_2O_3:Eu^{3+}$ > SiO_2 @ $Y_2O_3:Eu^{3+}$ > SiO_2 @ $Y_2O_3:Eu^{3+}$ @ SiO_2 at 254 nm. Similarly, the relative intensity of the emission spectrum at 612 nm is decreasing in order of $Y_2O_3:Eu^{3+}$ > SiO_2 @ $Y_2O_3:Eu^{3+}$ > SiO_2 @ $Y_2O_3:Eu^{3+}$ @ SiO_2, too. This may be related to the embeded structure of $Y_2O_3:Eu^{3+}$ in the core–shell particles, and attributed to the fact that the emitting volume of $Y_2O_3:Eu^{3+}$ is decreasing in the order of $Y_2O_3:Eu^{3+}$ > SiO_2 @ $Y_2O_3:Eu^{3+}$ > SiO_2 @ $Y_2O_3:Eu^{3+}$ @ SiO_2 [9,12,13]. This can be proved by the fact that the PL intensity of coating particle SiO_2 @ $Y_2O_3:Eu^{3+}$ even coating 4 number is yet less than that of pure $Y_2O_3:Eu^{3+}$ [9].

The literature investigation results showed that with the increase of amount of silica spheres, the PL intensities of the particles become weaker and weaker [26] due to the volume percentage of the interface is increased, which result the increase of the defects such as hanging M–O bonds, unexpected impurities, and imperfect crystals, and then these defects destroy the periodical arrangement of atoms, and many nonradiative centers are then formed in the interface. The enhancement of nonradiative relaxation will result in the obvious decrease of PL intensities.

While Lin and co-workers [9] give the result that the PL intensity of one layer $Y_2O_3:Eu^{3+}$ coated on SiO_2 particles increases with the increase of SiO_2 core particle size due to the decrease of surface defects and surface hanging bonds in larger particles because of their smaller surface area [27].

So the surface of $Y_2O_3:Eu^{3+}$ coated by SiO_2 will decrease the defects in the surface of the phosphor materials and enhance the emission intensity and efficiency of PL. But in this work the PL intensity of SiO_2 @ $Y_2O_3:Eu^{3+}$ @ SiO_2 is a little weaker than that of $Y_2O_3:Eu^{3+}$ and SiO_2 @ $Y_2O_3:Eu^{3+}$ material. This may be explained as that the emitting volume of $Y_2O_3:Eu^{3+}$ is decreased by coating another SiO_2 shell compared to the pure $Y_2O_3:Eu^{3+}$ and core–shell SiO_2 @ $Y_2O_3:Eu^{3+}$ [9,12,13]. It is believed that if we only coating SiO_2 shell on the $Y_2O_3:Eu^{3+}$ core, the PL intensity should be increased compared to that of SiO_2 @ $Y_2O_3:Eu^{3+}$ material. This is investigated in the next step.

On the other hand, the silica shell affecting the optical response of luminescing cores was recently investigated for two different mechanisms [28,29]. One is the influence of the coating was based on the reduction of the luminescence quenching of the surface hydroxil groups, and this enhancement of luminescence brought by coating strongly depends on the nature of the core [28]. It can be significant in the case of Mn-doped ZnS [28] or only slightly pronounced in Eu doped YVO_4 [30]. In some cases as pure Eu_2O_3 [31] or CdSe/ZnS [28], the luminescence is, on the contrary, found to be slightly decreased or severely dropped just like that in this study the emission intensity of SiO_2 @ $Y_2O_3:Eu^{3+}$@ SiO_2 is less than that SiO_2 @ $Y_2O_3:Eu^{3+}$. Another mechanism is explained that the luminescence enhancement of the core–shell naoparticles is due to the energy transfer between the two parts of a core–shell nanocomposite, the silica shell acting as an antenna which absorbs the light and transfers it to the core then enhancing the optical response [29]. But the latter mechanism was happened when the excitation wavelength is shorter than 250 nm because the silica is found to absorb significantly below 250 nm [32]. In this study, the energy transfer between SiO_2 shell and the core SiO_2 @ $Y_2O_3:Eu^{3+}$ composites did not found because the excitation wavelength is 254 nm which can not be absorbed well by SiO_2 shell.

4. Conclusions

In summary, we have demonstrated a simple approach for the synthesis of core–shell structure SiO_2 @ $Y_2O_3:Eu^{3+}$ and core–shell–shell particles like sandwich structure SiO_2 @ $Y_2O_3:Eu^{3+}$ @ SiO_2 with uniform size distribution and spherical morphology. Photoluminescence studies show that the existence of silica as core or shell have some extent affect on the luminescence property of $Y_2O_3:Eu^{3+}$ shell. One can change the size of SiO_2 core or $Y_2O_3:Eu^{3+}$ shell to obtain the best photoluminescence property.

References

[1] X. Teng, D. Black, N.J. Watkins, Y. Gao, H. Yang, Nano. Lett. 3 (2003) 261–263.
[2] Y. Yin, Y. Liu, B. Gates, Y. Xia, Chem. Mater. 13 (2001) 1146–1148.
[3] C. Graf, D.L.J. Vossen, A. Imhof, A. van Blaaderen, Langmuir 19 (2003) 6693–6700.
[4] T. Hase, T. Kano, E. Nakazawa, H.Y. Amamoto, Adv. Electron. Electron Phys. 79 (1990) 271–273.
[5] V.A. Bolchouchine, E.T. Goldburt, B.N. Levonovitch, V.N. Litchmanova, N.P. Sochtine, J. Lumin. 87/89 (2000) 1277–1280.
[6] G. Wakefield, E. Holland, P.J. Dobson, J.L. Hutchison, Adv. Mater. 13 (2001) 1557–1559.
[7] H. Wang, C.K. Lin, X.M. Liu, J. Lin, Appl. Phys. Lett. 87 (2005) 181907–181910.
[8] H.J. Feng, Y. Chen, F.Q. Tang, Mater. Lett. 60 (2006) 737–739.
[9] H. Wang, M. Yu, C.K. Lin, X.M. Liu, J. Lin, J. Phys. Chem. (C) 111 (2007) 11223–11230.
[10] K.Y. Jung, D.Y. Lee, Y.C. Kang, H.D. Park, J. Lumin. 105 (2003) 127–130.
[11] X. Jing, T.G. Ireland, C. Gibbons, D.J. Barber, J. Silver, A. Vecht, G. Fern, P. Trogwa, D. Morton, J. Electrochem. Soc. 146 (1999) 4546–4551.
[12] C.K. Lin, D.Y. Kong, X.M. Liu, H. Wang, M. Yu, J. Lin, Inorg. Chem. 46 (2007) 2674–2681.
[13] H. Wang, M. Yu, C.K. Lin, J. Lin, J. Colloid Interf. Sci. 300 (2006) 176–182.
[14] X.M. Liu, J. Lin, J. Nanopart Res. 9 (2007) 869–875.
[15] K.C. Barick, D. Bahadur, Bull. Mater. Sci. 29 (2006) 595–598.
[16] K. Aslan, M. Wu, R.J. Lakowicz, C.D. Geddes, J. Fluoresc. 17 (2007) 127–131.
[17] C. Graf, D.L.J. Vossen, A. Imhof, A.V. Blaaderen, Langmuir 19 (2003) 6693–6700.
[18] N. Liu, B.S. Prall, V.I. Klimov, J. Am. Chem. Soc. 128 (2006) 15362–15363.
[19] J.H. Kim, J.S. Kim, H. Choi, S.M. Lee, B.H. Jun, K.N. Yu, E. Kuk, Y.K. Kim, D.H. Jeong, M.H. Cho, Y.S. Lee, Anal. Chem. 78 (2006) 6967–6973.
[20] A.F. Gross, M.R. Diehl, K.C. Beverly, E.K. Richman, S.H. Tolbert, J. Phys. Chem. B 107 (2003) 5475–5482.
[21] K. Dick, T. Dhanasekaran, Z. Zhang, D. Meisel, J. Am. Chem. Soc. 124 (2002) 2312–2313.
[22] W. Stöber, A. Fink, E. Bohn, J. Colloid Interf. Sci. 26 (1968) 62–65.
[23] G.X. Liu, G.Y. Hong, D.X. Sun, J. Colloid Interf. Sci. 278 (2004) 133–138.
[24] D.K. Williams, B. Bihari, B.M. Tissue, J. Phys. Chem. B 102 (1998) 916–918.
[25] Y. Tao, G.W. Zhao, W.P. Zhang, S.D. Xia, Mater. Res. Bull. 32 (1997) 501–506.

[26] H.J. Feng, Y. Chen, F.Q. Tang, J. Ren, Mater. Lett. 60 (2006) 737–740.
[27] J. Dhanaraj, R. Jagannathan, T.R.N. Kutty, C.H. Lu, J. Phys. Chem. B 105 (2001) 11098–11100.
[28] D. Gerion, F. Pinaud, S.C. Williams, W.J. Parak, D. Zancher, S. Weiss, A.P. Alivisatos, J. Phys. Chem. B 105 (2001) 8861–8864.
[29] C. Louis, S. Roux, G. Ledoux, C. Dujardin, O. Tillemen, B.L. Cheng, P. Perriat, Chem. Phy. Lett. 429 (2006) 157–160.
[30] A. Huignard, V. Buissette, A.C. Franville, T. Gacoin, J.P. Boilot, J. Phys. Chem. B 107 (2003) 6754–6757.
[31] J. Feng, B.D. Hummock, I.M. Kennedy, G. Shan, A. Maqueira, US Patent 2003/0180780.
[32] B. Mercier, C. Dujardin, G. Ledoux, C. Louis, O. Tillement, P. Perriat, J. Appl. Phys. 96 (2004) 650–653.